RECEIVED 2000 JANUARY 21; ACCEPTED 2000 MARCH 13
Preprint typeset using LaTeX style emulateapj v. 26/01/00

CHANDRA X-RAY OBSERVATORY ARCSECOND IMAGING OF THE YOUNG, OXYGEN-RICH SUPERNOVA REMNANT 1E 0102.2-7219

T. J. GAETZ, YOUSAF M. BUTT, RICHARD J. EDGAR, KRISTOFFER A. ERIKSEN,
PAUL P. PLUCINSKY, ERIC M. SCHLEGEL, AND RANDALL K. SMITH
Harvard-Smithsonian Center for Astrophysics, 60 Garden Street, Cambridge, MA 02138

Received 2000 January 21; accepted 2000 March 13

ABSTRACT

We present observations of the young, oxygen-rich supernova remnant 1E 0102.2-7219 taken by the *Chandra X-ray Observatory* during its orbital activation and checkout phase. The boundary of the blast-wave shock is clearly seen for the first time, allowing the diameter of the remnant and the mean blast-wave velocity to be determined accurately. The prominent X-ray bright ring of material may be the result of the reverse shock encountering ejecta; the radial variation of O VII versus O VIII emission indicates an ionizing shock propagating inward, possibly through a strong density gradient in the ejecta. We compare the X-ray emission to Australia Telescope Compact Array 6 cm radio observations (Amy and Ball 1993) and to archival *Hubble Space Telescope* [O III] observations. The ring of radio emission is predominantly inward of the outer blast-wave, which is consistent with an interpretation of synchrotron radiation originating behind the blast-wave but outward of the bright X-ray ring of emission. Many (but not all) of the prominent optical filaments are seen to correspond to X-ray bright regions. We obtain an upper limit of $\sim 9 \times 10^{33}$ erg s^{-1} (3σ) on any potential pulsar X-ray emission from the central region.

Subject headings: Magellanic Clouds — shock waves — supernova remnants — X-rays: ISM

1. INTRODUCTION

The supernova remnant 1E 0102.2-7219 (hereafter E0102) in the Small Magellanic Cloud (SMC) is an interesting example of a young O-rich supernova remnant. It was first identified as a likely supernova remnant by Seward & Mitchel (1981) based on *Einstein* soft X-ray images of the SMC. Dopita, Tuohy, & Mathewson (1981) found a filamentary [O III] shell ($\sim$24″ diameter); the remnant was not visible in Hα ([O III]/Hβ $\gtrsim$60), and they classified the remnant as O-rich. They noted diffuse [O III] and Hα emission surrounding the [O III] filaments, with an emission "hole" of diameter $\sim$35–40″ surrounding the [O III], and suggested that the diameter of the hole could correspond to that of the blast-wave. In a follow-up spectroscopic study (Tuohy & Dopita 1983), O-rich material was found to have a full width velocity dispersion of $\sim$6500 km s^{-1}. If the O-rich material is assumed to be undecelerated ejecta, the 6.9 pc diameter of the [O III] emission (assuming a distance of 59 kpc) implies an age of $\sim$1000 yr. More recently, the remnant has been studied with the *Hubble Space Telescope* (Blair et al. 2000). The remnant has also been observed in the UV (Blair et al. 1989), radio (Amy & Ball 1993) and numerous times in the X-ray (Hayashi et al. 1994 and references therein). The X-ray spectrum of the remnant has proved difficult to understand; Hayashi et al. (1994) were unable to obtain a formally acceptable fit to the *ASCA* data, even with a rather complicated nonequilibrium ionization model, and concluded that the abundances in the plasma are inhomogeneous. By providing high spatial resolution, the *Chandra X-ray Observatory* will help us to solve these problems by reducing the spatial confusion that hampered earlier X-ray studies.

2. X-RAY DATA

We report here on observations of the supernova remnant E0102 obtained during the orbital activation and checkout period for the *Chandra X-ray Observatory* (Weisskopf, O'Dell, & van SpeyBroeck 1996). The data were obtained with the S3 chip of the Advanced CCD Imaging Spectrometer (ACIS; Garmire et al. 1992; Bautz et al. 1998), a backside-illuminated CCD with low to moderate spectral resolution ($E/\Delta E$ $\sim$4.3 at 0.5 keV, $\sim$31 at 5.9 keV). We analyzed observation Ids (ObsIds) 138 and 1231 (1999 Aug 23; processing version R4C3UPD2) and ObsId 1423 (1999 Nov 01; processing version R4CU4UPD1.1). The 138 and 1231 data were taken with a focal plane temperature of −100°C; the 1423 data were obtained at −110°C. The effective exposure times were 9759, 9762 and 19104 s (ObsIds 138, 1231, and 1423, respectively). We worked from *Chandra X-ray Observatory* Center (CXC) level 1 and level 2 event lists, and used the *ASCA*-like [0,2,3,4,6] grade set. The absolute sky coordinates derived from the FITS world coordinate system (E. W. Greisen & M. Calabretta 2000, in preparation) data in the event list headers yielded slightly different positions for the three data sets; ObsIds 138 and 1231 gave consistent results, but ObsId 1423 is shifted $\sim$1.″6 south-southeast relative to ObsId 138, consistent with a recently discovered secular drift in *Chandra* coordinate determinations between 1999 August and November. The 138 and 1231 data were taken within about a day of a boresight calibration observation and should be more accurate. We registered the three data sets against each other and applied the ObsId 138 coordinate transform. The event data were binned on 0.″492 pixels (ACIS pixels) and smoothed with a 0.″492 FWHM Gaussian (Fig. 1). We computed radial profiles based on 20° sectors and 0.″25 radial binning centered on α = 1$^{\rm h}$ 04$^{\rm m}$ 1.$^{\rm s}$94, δ = −72°01′52.″0 (J2000), the X-ray centroid.

The X-ray emission is dominated by a bright ring with a radius of $\sim$14″. The *Einstein* and *ROSAT* HRIs also detect evidence for a ring of emission, but with at least 5 times poorer spatial resolution, the remarkable substructure and brightness variations were not as evident as with *Chandra*. The ring is inhomogeneous and is brightest and spatially sharpest

($\lesssim$2″ FWHM) in the southeast, with significant knots south-southwest and west and a ridge northwest; the peak brightness varies by a factor of about 3 around the ring. The ring FWHM varies from ∼2″ to ∼8″ with mean ∼5″ (approximately half the total counts lie within the FWHM). The ring falls off most steeply toward the center, and more gradually outward with suggestions of irregularities or scalloping.

The remnant is bounded by a faint plateau with a relatively sharp outer edge, particularly in the northeast. This plateau shows a hint of limb brightening in the east and northeast; the southwest boundary is more diffuse and irregular. Interior to the bright ring the remnant is faint and patchy with suggestions of brighter ridges; a bright feature extends from near the center toward the bright region south-southwest.

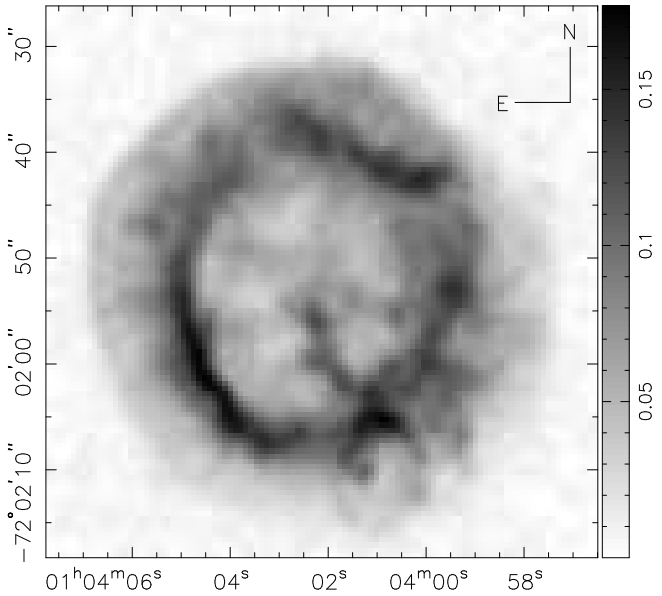

Fig. 1. — Grayscale image of the smoothed *Chandra* X-ray data (ObsIds 1423, 138, 1231); the square root of the intensity (in units of counts arcsec^{-2} s^{-1}) is plotted.

The backside-illuminated S3 chip has good low-energy detection efficiency, but the energy response is nonlinear and temperature-dependent, particularly below ∼1 keV; in view of the uncertainties in the response matrices at this stage of the calibration, we defer a detailed spectral investigation and abundance determination. Nevertheless, the energy scales are sufficiently accurate to allow identification of the major spectral features seen in the earlier *ASCA* data, and for qualitative assessments to be made. In Figure 2 , we plot the pulse-height amplitude (PHA) spectrum for the remnant as a whole (combined ObsIds 138 and 1231).

We have examined a number of spectra extracted from various regions in the remnant including the outer shock region, regions of the bright ring, and brighter and fainter regions interior to the bright ring. The spectra vary throughout the remnant. The O and Ne lines are less prominent in the outer shock region; the O and Ne seem to be in a higher excitation state with much of the emission coming from the H-like stages. The plasma state (e.g., the ratio of the He-like to H-like O [and Ne]) also varies around the bright ring.

In order to get a better idea of the variation of plasma conditions within the remnant, we constructed difference maps based on bands centered around the prominent emission lines: ∼0.46 – 0.61 keV (O VII He-like triplet), ∼0.61 – 0.72 keV (O VIII Lyα), ∼0.86 – 0.98 keV (Ne IX He-like triplet), and ∼0.98 – 1.10 keV (Ne X Lyα). In Figure 3 we plot a difference image of the bands dominated by the O VIII Ly α line and the O VII He-like triplet; in Figure 4 we show radial profiles for a 20° sector centered 40° south of east (i.e., position angle 130°).

Hughes (1988, 1994) ruled out a simple uniform-density shell model for the X-ray emission on the basis of the (much lower resolution) *Einstein* and *ROSAT* HRI data. The *Chandra* data also suggest that the X-ray morphology is more complex than a uniform shell. In the top panel of Figure 4, we plot the azimuthally averaged X-ray profile and a best fit uniform shell model. Overall, the *Chandra* data suggest a faint shell of X-ray emission surrounding a bright inhomogeneous ring of emission, possibly thin and ribbon-like. The X-ray remnant as a whole is remarkably round (∼10% longer northeast to southwest than northwest to southeast). The mean X-ray diameter is ∼44″. At a distance of 59 kpc, this corresponds to a linear diameter of ∼12.6 pc; for an assumed remnant age of ∼1000 yr, the mean blast-wave velocity is ∼6200 km s^{-1}.

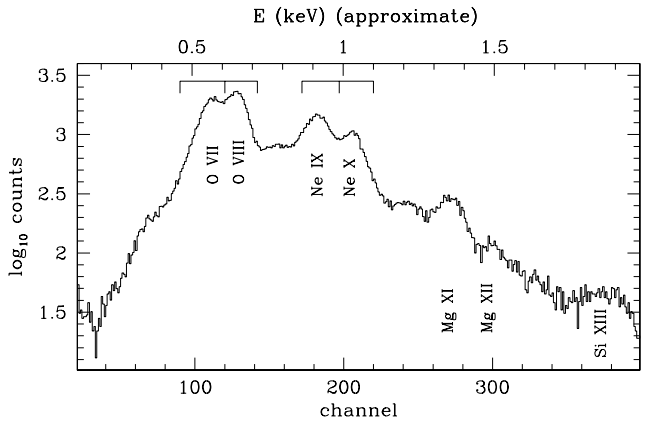

Fig. 2. — *Chandra* low energy PHA spectrum for the whole remnant (ObsIds 138 + 1231). The upper axis is labeled with an *approximate* energy scale. We also show the locations of the O VII, O VIII, Ne IX, and Ne X-dominated bands (for T_{fp} = −100° C; see text). The approximate locations of the Lyα H-like and He-like triplet lines of O, Ne, Mg, and Si are indicated.

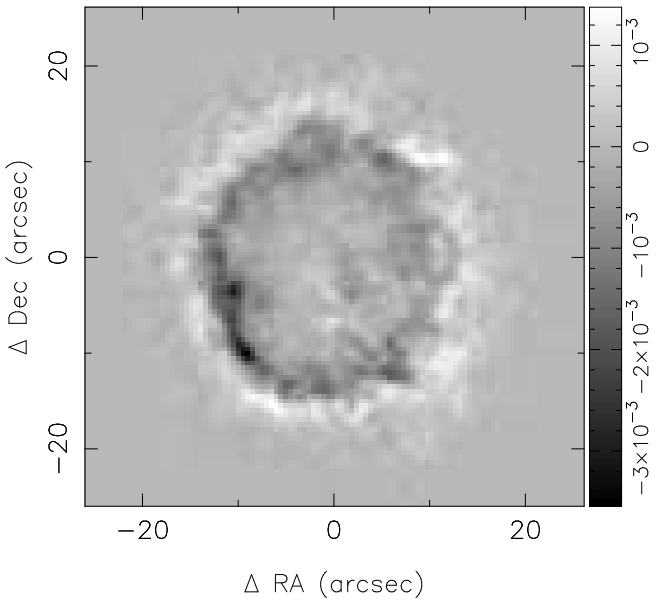

Fig. 3. — Difference image of bands centered on the O VIII Ly α line and the O VII He-like triplet. O VIII is white, and O VII is black (in units of counts arcsec^{-2} s^{-1})

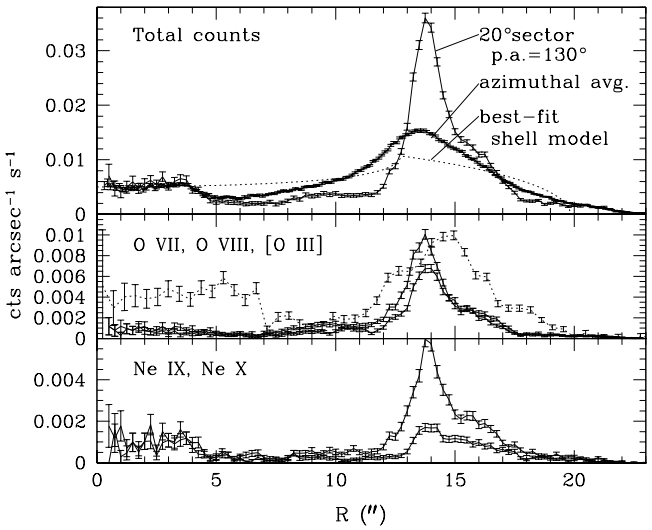

Fig. 4. — Radial profiles for a 20°-wide sector centered at position angle 130 (40° south of east; the narrowest and brightest portion of the X-ray ring). *Top*: Total count rate for the 20° sector. For reference, an azimuthal average over the remnant is shown, together with the best fit (χ^2/dof = 230) uniform shell model for the azimuthal average. *Middle*: O VII (*upper curve*), O VIII (*lower curve*), [O III] flux (arbitrary scale, *dotted curve*) (see §4. *Bottom*: Ne IX (*upper curve*), Ne X (*lower curve*).

3. COMPARISON WITH 6 CM RADIO OBSERVATIONS

Amy & Ball (1993) observed the remnant with 3″ resolution at 6 cm using the Australia Telescope Compact Array (ATCA), and found an outer shell of radio emission with diameter $40'' \pm 5''$. They note that this matches the size of the [O III] and Hα "emission hole" of Dopita et al. (1981) and the X-ray emission (*Einstein* HRI). In Figure 5, we plot radio contours on the *Chandra* X-ray image. The radio ring maps out the outer X-ray emission well, including the slight northeast to southwest elongation; the radio ring lies predominantly outside the bright X-ray ring but within the outer X-ray rim. The radio emission is brightest in the northeast, just inside the brightest portion of the outer X-ray limb. The radio ring weakens toward the southeast, where the X-ray ring is sharpest and brightest. However, in the northwest, a bright radio ridge wraps somewhat around the brightest portion of an X-ray ridge and a region of enhanced [O III] emission (see also §4). In the southwest, a local enhancement of the radio emission corresponds to a local X-ray enhancement, while the optical data indicate a corresponding gap in the [O II] and [O III] emission.

Amy & Ball (1993) noted a central enhancement in the 6 cm data and suggested the possibility of a plerionic component (acknowledging the possibility that it was a mere projection effect). At the level of the available *Chandra* aspect solution, the central radio enhancement overlaps a central X-ray bright knot. In the X-ray data, this knot coincides with part of a bright ridge extending to the south (faintly visible in the radio data as well), making it likely that the enhancement is a chance superposition. We obtain an X-ray upper limit on any plerionic contribution as follows: After background subtraction, the number of counts above $\sim$3 keV and within 10″ of the center of the remnant is 30 ± 11 counts in a 9762 s exposure, or $\sim(3.1 \pm 1.1) \times 10^{-3}$ counts s^{-1}. Using an adopted Crab spectrum (with a power-law of index 2.05), the prelaunch response matrix for the S3 chip, and the assumed distance of 59 kpc, the 3σ upper limit is $\sim 9 \times 10^{33}$ erg s^{-1}.

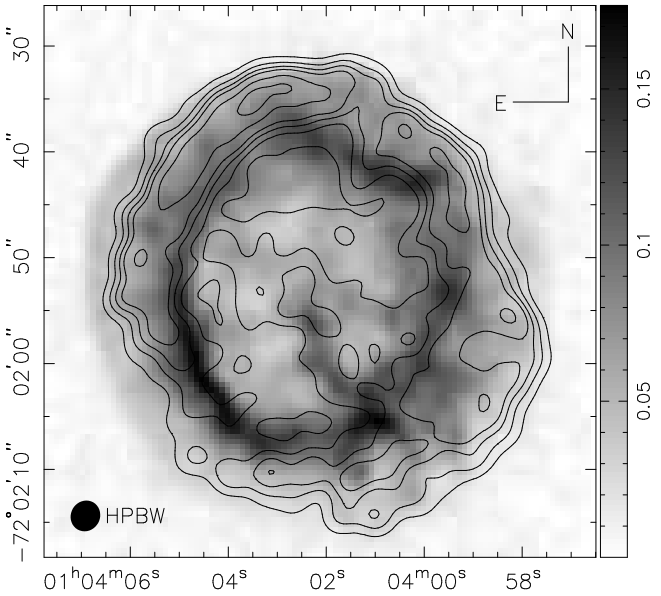

Fig. 5. — *Chandra* X-ray data with ATCA 6 cm radio contours. The X-ray gray scale is the same as in Fig. 1. The radio contours are 0.25, 0.5, 0.75, 1, 1.5, 2, 2.5, and 3 mJy beam^{-1}; the rms noise is $\sim 7.5 \times 10^{-2}$ mJy beam^{-1} (Amy & Ball 1993).

4. COMPARISON WITH OPTICAL DATA

We examined *Hubble Space Telescope* (*HST*) archival [O III] images of the remnant. Figure 6 is a composite color image of the remnant with the 6 cm radio data in red, the *HST* [O III] data in green, and the *Chandra* X-ray data in light blue. The *Chandra* absolute coordinates are currently uncertain at a level of at least $\sim 1''$ (see §2).

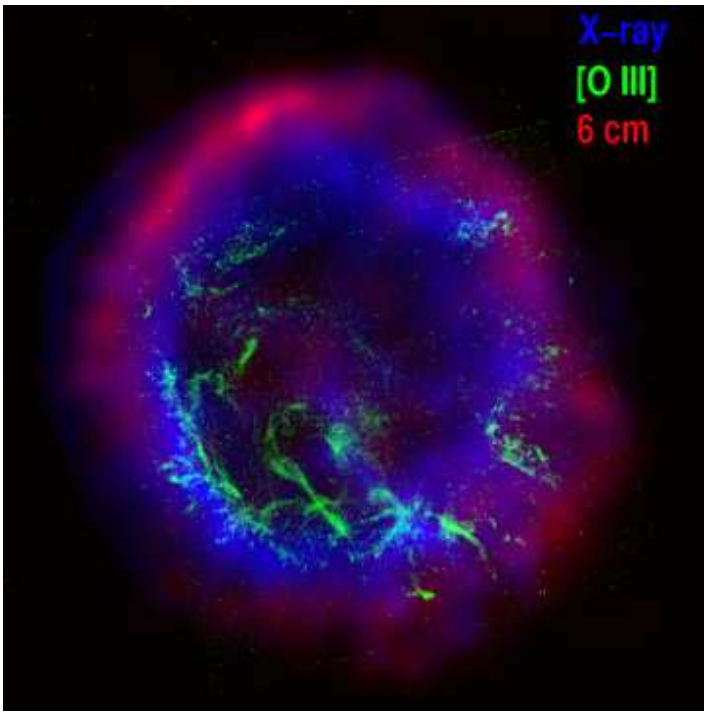

Fig. 6. — Color composite image of the ATCA 6 cm radio data (red), *HST* [O III] data (green), and *Chandra* X-ray data (light blue).

The southeast portion bright X-ray ring coincides with a series of [O III] filaments, sharply bounded toward the center of

the remnant, with knots and filaments extending outward. This suggests that we are seeing a tangency of a shock propagating through ejecta. The [O III] knots could be engulfed dense ejecta clumps or Rayleigh-Taylor fingers of ejecta; the optical emission could be produced by shocks driven into cooler, denser material by the high pressure downstream of the reverse shock, or by photoionization and excitation by the X-rays from the surrounding material (Dopita, Binette, & Tuohy 1984; Blair et al. 1989). Note that the [O III] data were obtained with the Planetary Camera of the *HST* using the F502N filter. This filter is narrow enough that significant emission may be Doppler-shifted out of the filter band pass, particularly for filaments projected toward the interior on the front and back faces of an expanding shell (Blair et al. 2000). The inner edges of the southeast [O III] filaments may lie inward of the X-ray ring by $\sim 1''$ (Fig. 4); however, elsewhere in the remnant, bright [O III] knots coincident with bright X-ray features also tend to be slightly westward of the X-ray emission. This may also be in part a result of the *Chandra* absolute coordinate uncertainty.

A number of bright X-ray knots west through south coincide with optically bright features; most notably, the bright X-ray knot in the south-southwest is likely related to the bright [O III] filament, the brightest [O III] feature in the remnant. Bright [O III] filaments border a remarkable gap in the southwest that is suggestive of a blowout. The X-ray ring is particularly broad at this point, and the radio shows an enhancement as well. As noted above, the outer shock in the southwest quadrant is more ragged and less well defined.

The brightest part of the X-ray ridge in the northwest also coincides with enhanced [O III] emission. It is also notable that the 6 cm radio emission shows a ridge in the same location, cupped around the X-ray and optically bright emission; the morphology suggests a denser clump of ejecta being engulfed by the reverse shock.

There are also puzzling differences between the optical [O III] and X-ray emission; for example, an optical filament in the southeast (between the central spoke and the ring) is not associated with enhanced X-ray emission. It is also notable that the X-ray and radio emission look like complete (if nonuniform) rings approximately in the plane of the sky, while the optical emission shows, at best, an incomplete ring with large gaps (*e.g.*, north, west, southwest); Tuohy & Dopita (1983) modeled the [O II] emission and velocity distribution as an extremely distorted ring perpendicular to the plane of the sky.

5. DISCUSSION

It is plausible to identify the sharp outer edge of the X-ray emission as the location of the direct blast-wave interacting with the ambient medium and the inner edge of the bright ring as the reverse shock. The scalloping in the region between the bright ring and the rim might then be the result of Rayleigh-Taylor instabilities of the contact surface. The outer shock is brightest in the northeast, and at least 5 times fainter in the southwest. The nonthermal radio emission would be synchrotron emission originating behind the main blast-wave. The bright radio ridge in the northeast, corresponding to the brightest section of the outer X-ray shock, together with the slight elongation northeast to southwest elongation of the remnant suggests that the ambient medium may be slightly stratified in that direction.

In the X-ray difference maps (e.g., Fig. 3), the remnant shows a clear layered morphology, in which the inner edge of the bright ring is enhanced in O VII emission, while the outer part is enhanced in O VIII. The Ne IX and Ne X emission shows a similar pattern with Ne IX more prominent near the inner edge. The Ne emission is relatively more prominent outward of the peak in the O VII-dominated band. This pattern suggests that we are seeing the ionization of the gas which has passed through the reverse shock. The southeast portion of the ring is particularly interesting in this regard, being much brighter and narrower than the rest of the ring; Figure 4 shows radial profiles through this portion of the remnant. The steep rise at the inner edge and the lag of O VIII relative to O VII are suggestive of a reverse shock, possibly propagating through a steep density gradient.

In summary, the *Chandra* observations have allowed us to detect the outer blast wave for the first time, and to determine accurately the size of the remnant; the ring of radio emission is predominantly inward of the X-ray blast wave, which is consistent with an interpretation as synchrotron radiation originating behind the blast wave, but outward of the bright X-ray ring of emission. Complex variations are seen in the bright X-ray ring. The X-ray spectra vary throughout the remnant. Difference images centered on the prominent H-like and He-like lines of O and Ne suggest that the bright ring corresponds to an ionizing reverse shock. Many (but not all) of the prominent optical filaments are seen to correspond to X-ray bright regions.

We thank Shaun Amy and Lewis Ball for making available their published 6 cm data. We also thank the referee, Jon Morse, for suggestions which markedly improved this article. This work was supported by NASA contract NAS8-39073, and in part by NASA LTSA NAG5-3559.

REFERENCES

Amy, S. W., & Ball, L. 1993, ApJ, 411, 812
Bautz, M. W., *et al.* 1998, X-Ray Optics, Instruments and Missions, ed. R. B. Hoover & A. B. Walker, Proc. SPIE, 3444, 210
Blair, W. P., Raymond, J. C., Danziger, J., & Matteucci, F. 1989, ApJ, 338, 812
Blair, W. P., *et al.* 2000, ApJ, in press.
Dopita, M. A., Binette, L, & Tuohy, I. R. 1984, ApJ, 282, 142
Dopita, M. A., Tuohy, I. R., & Mathewson, D. S. 1981, ApJ, 248, 105
Garmire, G. P. *et al.* 1992, AIAA, Space Programs and Technologies Conference, Huntsville, AL, Mar. 24-27.
Hayashi, I., Koyama, K., Masanobu, O., Miyata, E., Tsunemi, H., Hughes, J. P., & Petre, R. 1994, PASJ, 46, L121
Hughes, J. P. 1988, in Supernova Remnant and the Interstellar Medium, eds. R. S. Roger & T. L. Landecker (Cambridge: Cambridge Univ. Press), 125
Hughes, J. P. 1994, in The Soft X-ray Cosmos, AIP Conf. Proc. 313, eds. E. M. Schlegel & R. Petre (New York: AIP), 144
Seward, F. D., & Mitchel, M. 1981, ApJ, 243, 736
Tuohy, I. R., & Dopita, M. A. 1983, ApJ, 268, 11
Weisskopf, M. C., O'Dell, S. L., & van Speybroeck, L. P. 1996, Proc. SPIE, 2805, 2